

# Unit conversion in pseudopotential lattice Boltzmann method for liquid–vapor phase change simulations

Cite as: Phys. Fluids **34**, 103305 (2022); <https://doi.org/10.1063/5.0106079>

Submitted: 27 June 2022 • Accepted: 06 September 2022 • Accepted Manuscript Online: 08 September 2022 • Published Online: 05 October 2022

 Si-Cheng Wang (汪思成),  Zi-Xiang Tong (董自翔), Ya-Ling He (何雅玲), et al.



View Online



Export Citation



CrossMark

## ARTICLES YOU MAY BE INTERESTED IN

[Lattice Boltzmann modeling and simulation of forced-convection boiling on a cylinder](#)

Physics of Fluids **33**, 023307 (2021); <https://doi.org/10.1063/5.0032743>

[Mesoscopic simulation of three-dimensional pool boiling based on a phase-change cascaded lattice Boltzmann method](#)

Physics of Fluids **32**, 103312 (2020); <https://doi.org/10.1063/5.0023639>

[Mesoscopic modeling of vapor cavitation bubbles collapse and interaction in near-wall region with a pseudopotential lattice Boltzmann method](#)

Physics of Fluids **34**, 092012 (2022); <https://doi.org/10.1063/5.0099989>



## Physics of Fluids

### Special Topic: Food Physics

Submit Today!

# Unit conversion in pseudopotential lattice Boltzmann method for liquid–vapor phase change simulations

Cite as: Phys. Fluids **34**, 103305 (2022); doi: [10.1063/5.0106079](https://doi.org/10.1063/5.0106079)

Submitted: 27 June 2022 · Accepted: 6 September 2022 ·

Published Online: 5 October 2022





View Online



Export Citation



CrossMark

Si-Cheng Wang (汪思成),  Zi-Xiang Tong (童自翔), <sup>a)</sup>  Ya-Ling He (何雅玲), and Xiang Liu (刘翔)

## AFFILIATIONS

Key Laboratory of Thermo-Fluid Science and Engineering of Ministry of Education, School of Energy and Power Engineering, Xi'an Jiaotong University, Xi'an, Shaanxi 710049, China

<sup>a)</sup> Author to whom correspondence should be addressed: [zxtong@xjtu.edu.cn](mailto:zxtong@xjtu.edu.cn)

## ABSTRACT

Pseudopotential lattice Boltzmann (LB) model is an effective mesoscopic method for liquid–vapor phase change simulations. In LB methods, calculations are often carried out in lattice units. Thus, a correct mapping from the lattice unit system to the physical unit system is crucial for accurate simulations of practical problems. The unit conversion for liquid–vapor phase change problems is more complicated than single-phase problems, because an equation of state (EOS) for a nonideal fluid is introduced in the pseudopotential two-phase model. In this work, a novel unit conversion method for the pseudopotential LB model is proposed. The basic strategy is to obtain the conversion relations of fundamental units by mapping the surface tension and EOS parameters related to fluid properties, and thus, the unit conversion relations of other quantities are deduced. Numerical simulations of benchmark problems including the film evaporation and the bubble heterogeneous nucleation from a V-shaped cavity are carried out, and the simulation results are converted to the physical unit system by the proposed method. The numerical results demonstrate that the proposed method is able to recover the physical-unit latent heat of the fluid in the film evaporation problem. In the bubble nucleation from a V-shaped cavity problem, the conventional unit conversion method cannot derive the correct superheat temperature in the physical unit, whereas the proposed method based on the fundamental units recovers the critical superheat temperature which is consistent with the analytical result.

Published under an exclusive license by AIP Publishing. <https://doi.org/10.1063/5.0106079>

## I. INTRODUCTION

Liquid–vapor phase change, especially boiling, is an efficient mode of heat transfer. It has a wide range of industrial applications such as the heat dissipation of power electronic chips and nuclear reactors.<sup>1–4</sup> Numerical simulation is an important approach on studying the process and mechanism of boiling heat transfer. Conventional multiphase flow numerical methods for boiling mainly include the level set method<sup>5</sup> and the volume of fluid method,<sup>6</sup> which are all macroscopic approaches based on solving the Navier–Stokes equations and the energy equation directly.<sup>7</sup> In those macroscopic methods, interface reconstruction or re-initialization procedures are usually required, which can be time-consuming or not always physically consistent.<sup>8</sup> Moreover, when simulating the boiling heat transfer problem, parameters such as initial bubble nucleation sites and the waiting period of a newly nucleating bubble need to be assumed in those methods.<sup>9,10</sup> In recent years, the multiphase lattice Boltzmann method (LBM) has been successfully employed in boiling heat transfer simulations.

When compared with conventional macroscopic methods, the LBM is a mesoscopic method based on the Boltzmann equation,<sup>11</sup> which simulates the flow field through the evolution of virtual particles. This particle feature of the lattice Boltzmann (LB) model gives it the advantage in modeling boiling phase change phenomena. For example, by introducing mimetic interparticle forces, the Shan–Chen pseudopotential multiphase LB model could generate phase separations automatically without any interface tracking or capturing algorithms, which are indispensable in macroscopic approaches.<sup>12,13</sup> Moreover, the bubble nucleation and growth are also automatic in pseudopotential boiling simulations, while no artificial assumptions of the bubble nucleation parameters are required. Thus, the boiling curve in different stages (nucleate boiling, transition boiling, and film boiling) could be obtained naturally.<sup>14</sup> Compared with other multiphase LB models such as the free-energy model and the color-gradient model, the pseudopotential LB model is simple to implement, and an equation of state (EOS) can be introduced for the thermodynamic relation during phase

change.<sup>12</sup> Therefore, the pseudopotential LB is widely employed in boiling heat transfer simulations.<sup>9,15–21</sup>

Calculations in LB simulations are usually carried out in the form of a lattice unit system. For general flow and heat transfer problems, the lattice unit system includes four fundamental units, which are lattice length unit (lu), lattice mass unit (mu), lattice time step (ts), and lattice temperature unit (tu). However, practical problems often need to be presented in the form of a physical unit system (e.g., SI system). Therefore, a correct mapping from the lattice unit system to the physical unit system is crucial for the application of LB models.

Conventional unit conversion methods are based on the mapping of dimensionless parameters and the principle of corresponding state.<sup>22,23</sup>

The former method matches a set of dimensionless parameters related to the concerned physical problem based on the Buckingham  $\pi$  theorem, and some parameters in the LB simulations (such as the relaxation time) are determined.<sup>11,24</sup> The latter links the physical units and the lattice units by the reduced properties in the EOS. The reduced property is defined as the original property divided by the critical property, for example,  $\rho_R = \rho/\rho_c$ ,  $T_R = T/T_c$ . According to the principle of corresponding state, the reduced properties should be the same under any kind of unit system.<sup>25</sup> In recent pseudopotential LBM boiling studies, the conversion method based on dimensionless parameters is often implemented combined with the principle of corresponding state. Table I summarizes some of the boiling studies using the pseudopotential

TABLE I. Literature review of boiling simulations using LB model and ways of variable representation.

Authors and published year	Numerical methods and simulation conditions	Ways of variable representation
Fang <i>et al.</i> <sup>9</sup>	Multi-relaxation-time (MRT) pseudopotential model coupled with thermal LB model. P–R EOS, $a = 0.02267$ , $b = 2/21$ , $R = 1$ . Pool boiling on a plain surface and on a cavity at saturated temperature $T_s = 0.86T_c$ and $T_s = 0.68T_c$ .	Time, length, and heat flux represented in lattice unit. Absolute temperature given in the reduced form $T_R = T/T_c$ . Superheat nondimensionalized as $Ja$ .
Mu <i>et al.</i> <sup>15</sup>	MRT pseudopotential model coupled with thermal LB model. P–R EOS, $a = 3/49$ , $b = 2/21$ , $R = 1$ . Pool boiling on cavities of various shapes at $T_s = 0.86T_c$ .	Time, length, and heat flux all represented in SI unit. Unit conversion process not clarified.
Sayyari and Esfahani <sup>16</sup>	MRT pseudopotential model coupled with thermal LB model. P–R EOS, $a = 3/49$ , $b = 2/21$ , $R = 1$ . Pool boiling on a platform heater at $T_s = 0.86T_c$ .	Time and length nondimensionalized by characteristic values $t_0$ and $l_0$ , $t^* = t/t_0$ , $l^* = l/l_0$ . Heat flux given in lattice unit. Heat transfer coefficient (HTC) nondimensionalized as $Nu$ . Superheat nondimensionalized as $Ja$ . Absolute temperature given in the reduced form $T_R$ .
Zhang <i>et al.</i> <sup>17</sup>	MRT pseudopotential model coupled with finite difference model (FDM) for heat transfer solved in the fourth-order Runge–Kutta scheme. P–R EOS, $a = 3/49$ , $b = 2/21$ , $R = 1$ . Pool boiling on a rectangular convex heater at $T_s = 0.86T_c$ .	Time and length nondimensionalized by characteristic values $t_0$ and $l_0$ , $t^* = t/t_0$ , $l^* = l/l_0$ . Superheat nondimensionalized as $Ja$ .
Chang <i>et al.</i> <sup>18</sup>	Bhatnagar–Gross–Krook (BGK) pseudopotential model coupled with FDM for heat transfer solved in the second-order Runge–Kutta scheme. P–R EOS, $a = 1/49$ , $b = 2/21$ , $R = 1$ . Pooling boiling on a plain surface and structured surfaces with columns at $T_s = 0.85T_c$ .	Time and length nondimensionalized by characteristic values $t_0$ and $l_0$ , $t^* = t/t_0$ , $l^* = l/l_0$ . Heat flux given in lattice unit. Absolute temperature and superheat given in the reduced form. Surface tension nondimensionalized as $Ca = \rho_L \nu_L u_0 / \sigma$ , where $u_0 = \sqrt{g l_0}$ .
Ma and Cheng <sup>19</sup>	MRT pseudopotential model coupled with thermal LB model. P–R EOS, $a = 2/49$ , $b = 2/21$ , $R = 1$ . Pool boiling on a plain surface and a rectangular heater at $T_s = 0.9T_c$ .	Time and length nondimensionalized by characteristic values $t_0$ and $l_0$ , $t^* = t/t_0$ , $l^* = l/l_0$ . Heat flux given in dimensionless form $q^* = q/q_{bo}$ , where the reference heat flux defined as $q_{bo} = \mu_L h_{fg} / l_0$ . Absolute temperature given in the reduced form $T_R$ . Superheat nondimensionalized as $Ja$ .
Zhang <i>et al.</i> <sup>20</sup>	MRT pseudopotential model coupled with thermal LB model. P–R EOS, $a = 3/49$ , $b = 2/21$ , $R = 1$ . Flow boiling in a vertical pipe with a diameter of 3 mm at $T_s = 0.91T_c$ .	Given the lattice–physical unit conversion results of length, kinematic viscosity, temperature, and density, the conversion process is not clarified. Time and length values nondimensionalized by characteristic values $t_0$ and $l_0$ in discussion. HTC nondimensionalized as $Nu$ . Heat flux given in lattice unit. Superheat nondimensionalized as $Ja$ .
Chen <i>et al.</i> <sup>21</sup>	MRT pseudopotential model coupled with thermal LB model. P–R EOS, $a = 2/49$ , $b = 2/21$ , $R = 1$ . Flow boiling in a horizontal pipe with a diameter of 4 mm at $T_s = 0.88T_c$ .	Time and length nondimensionalized by characteristic values $t_0$ and $l_0$ , $t^* = t/t_0$ , $l^* = l/l_0$ . Heat flux given in dimensionless form $q^* = q/q_f$ where the reference heat flux defined as $q_f = G_L h_{fg}$ , where $G_L$ is the inlet mass flow rate. Absolute temperature given in the reduced form $T_R$ . Superheat nondimensionalized as $Ja$ .

multiphase LBM in the recent 5 yr. The numerical models, simulation conditions, and the ways of variable representation in their results are listed. As shown in Table I, the characteristic length defined by the capillary length  $l_0 = \sqrt{\sigma/g(\rho_L - \rho_V)}$  and the characteristic time  $t_0 = \sqrt{l_0/g}$  defined correspondingly are widely used in the nondimensionalization of the length and time values.<sup>9,16–21</sup> Absolute temperatures are represented in their reduced form.<sup>9,15–21</sup> Other dimensionless numbers such as the Nusselt number ( $Nu$ ), Jakob number ( $Ja$ ), and nondimensional heat flux derived from lattice-unit quantities are chosen to describe and quantify the boiling processes.<sup>9,16,17,19–21</sup> The values in dimensionless forms are just intermediate results of the lattice-to-physical unit conversion. In the previous pseudopotential LB boiling studies, however, complete procedures of the unit conversion have rarely been discussed.

The conventional unit conversion method requires a set of dimensionless numbers related to the problem. However, the choice of such dimensionless numbers can be complicated for some practical physical problems.<sup>23</sup> In recent years, some more general methods have been proposed for the unit conversion in LBM. Huang *et al.*<sup>22</sup> developed a general approach for unit conversion for single-phase flow and validated the model by a two-dimensional (2D) problem of convective heat transfer in tube banks. Baakeem *et al.*<sup>23</sup> proposed a method to convert the units by determining the values of base quantities in the lattice unit system and the physical unit system, respectively. The unit conversion of a two-phase problem was implemented in their work. However, the derivation of the base quantities for the two-phase problem was not elucidated. Tong *et al.*<sup>26</sup> did the unit conversion from a lattice unit system to a molecular dynamics (MD) unit system in their LBM/MD coupled model for two-phase flows by matching the EOS in pseudopotential LBM with the EOS of MD. The length, velocity, and density ratios were matched, but the matching of surface tension was not considered. Recently, Jaramillo *et al.*<sup>27</sup> discussed the scaling process of lattice units in a mesh refinement procedure in two-phase LB simulations. The matching of critical parameters in the EOS and the surface tension is considered. The work focused on the unit scaling between lattice systems with different grid sizes, and the conversion to the physical unit system was not discussed. When compared with single-phase LB models, the unit conversion in the liquid–vapor phase change pseudopotential LB model is more complicated because the EOS related to the fluid property is introduced to the model and the matching of surface tension should be considered. Thus, the mapping of absolute temperature and pressure is required in unit conversion. In this work, we aimed to develop a novel unit conversion method based on the conversion of the fundamental units. Taking the mapping of EOS parameters and surface tension as constraints, the phase change simulation results in pseudopotential LB calculations can be accurately converted back to the physical unit system.

The rest of this paper is organized as follows: In Sec. II, the pseudopotential LB model for liquid–vapor phase change simulation is briefly introduced. The detailed lattice-to-physical unit conversion procedures are presented, which include the conventional unit conversion method based on the dimensionless parameter correspondence and the principle of corresponding state, as well as the novel method based on the fundamental unit conversion. The LB model used in this paper is verified in the form of lattice units in Sec. III. The unit conversion methods are implemented in Sec. IV, and the simulation results in the form of physical units are discussed. Finally, some conclusions are given in Sec. V.

## II. NUMERICAL METHOD

### A. The hybrid thermal LB model for phase change

In this study, the hybrid thermal LB model is applied to simulate liquid–vapor phase change, which consists of the pseudopotential LB model for multiphase flow and the finite difference model (FDM) for heat transfer process.<sup>14</sup> The multi-relaxation-time (MRT) collision operator is employed in the two-phase flow field simulation. When compared with the single-relaxation-time (SRT) model, the MRT model has better numerical stability because it has more independently adjustable relaxation parameters.<sup>28</sup> A source term can also be added in the MRT model to achieve tunable surface tension.<sup>29</sup> The evolution equation of the density distribution function is given as

$$f_\alpha(\mathbf{x} + \mathbf{e}_\alpha \delta_t, t + \delta_t) - f_\alpha(\mathbf{x}, t) = -\hat{\Lambda}_{\alpha\beta} [f_\beta(\mathbf{x}, t) - f_\beta^{\text{eq}}(\mathbf{x}, t)] + \delta_t (G_\alpha(\mathbf{x}, t) - 0.5 \hat{\Lambda}_{\alpha\beta} G_\beta(\mathbf{x}, t)), \quad (1)$$

where  $f_\alpha(\mathbf{x}, t)$  is the density distribution function in the  $\alpha$ th lattice direction at position  $\mathbf{x}$  and time  $t$ ;  $f_\alpha^{\text{eq}}(\mathbf{x}, t)$  is the equilibrium distribution function;  $\mathbf{e}_\alpha$  is the discrete velocity;  $\mathbf{G}$  represents the forcing term in velocity space, which is related to the force  $\mathbf{F}$  applied on each lattice; and  $\hat{\Lambda}$  is the MRT collision matrix. The subscript  $\beta$  follows the Einstein summation notation, that is, two repeated indexes imply taking the summation over this index. The D2Q9 lattice model is used in this study, and the discrete velocity vector is given by<sup>30</sup>

$$\mathbf{e} = c \begin{bmatrix} 0 & 1 & 0 & -1 & 0 & 1 & -1 & -1 & 1 \\ 0 & 0 & 1 & 0 & -1 & 1 & 1 & -1 & -1 \end{bmatrix}, \quad (2)$$

where  $c = \delta_x/\delta_t$  is the lattice speed. Because the unit conversion is independent of the dimension and the velocity discrete scheme, the unit conversion method developed in this work can be also used in 3D problems and other DdQq lattice Boltzmann models.

Using an orthogonal transformation matrix  $\mathbf{M}$ , the right-hand side of Eq. (1) can be transformed to a collision in the moment space

$$\mathbf{m}' = \mathbf{m} - \Lambda(\mathbf{m} - \mathbf{m}^{\text{eq}}) + \delta_t \left( \mathbf{I} - \frac{\Lambda}{2} \right) \mathbf{S}, \quad (3)$$

where  $\mathbf{m} = \mathbf{M}\mathbf{f}$ ,  $\mathbf{m}^{\text{eq}} = \mathbf{M}\mathbf{f}^{\text{eq}}$ ,  $\mathbf{S} = \mathbf{M}\mathbf{G}$ ,  $\Lambda = \mathbf{M}\hat{\Lambda}\mathbf{M}^{-1}$ ,  $\mathbf{I}$  is the unit matrix, and  $\mathbf{m}'$  is the moment after collision. For the D2Q9 model, the definition of the orthogonal transformation matrix  $\mathbf{M}$  can be found in Ref. 31.  $\Lambda$  is a diagonal matrix that contains multiple relaxation times and is given by<sup>32</sup>

$$\Lambda = \text{diag}(\tau_\rho^{-1}, \tau_e^{-1}, \tau_\zeta^{-1}, \tau_j^{-1}, \tau_q^{-1}, \tau_j^{-1}, \tau_q^{-1}, \tau_\nu^{-1}, \tau_\nu^{-1}), \quad (4)$$

where  $\tau_\nu$  is the relaxation time related to the kinematic viscosity,  $\nu = c_s^2(\tau_\nu - 0.5)\delta_t$ . The equilibrium distribution function in the moment space is given by<sup>32</sup>

$$\mathbf{m}^{\text{eq}} = \mathbf{M}\mathbf{f}^{\text{eq}} = \rho(1, -2 + 3|\mathbf{u}|^2, 1 - 3|\mathbf{u}|^2, u_x, -u_x, u_y, -u_y, u_x^2 - u_y^2, u_x u_y)^T. \quad (5)$$

After the collision process in the moment space, the distribution function is then transformed back to the velocity space for the streaming process

$$f_\alpha(\mathbf{x} + \mathbf{e}_\alpha \delta_t, t + \delta_t) = f'_\alpha(\mathbf{x}, t), \quad (6)$$

where  $f'$  is the post-collision distribution function,  $\mathbf{f}' = \mathbf{M}^{-1}\mathbf{m}'$ . The macroscopic density and velocity are recovered by<sup>33</sup>

$$\rho = \sum_{\alpha} f_{\alpha}, \quad \rho \mathbf{u} = \sum_{\alpha} \mathbf{e}_{\alpha} f_{\alpha} + \frac{\delta_t}{2} \mathbf{F}. \quad (7)$$

The improved forcing scheme proposed by Li *et al.*<sup>32</sup> is employed for the forcing term  $\mathbf{S}$  in the moment space, which can improve the thermodynamic consistency

$$\mathbf{S} = \begin{bmatrix} 0 \\ 6\mathbf{u} \cdot \mathbf{F} + \frac{12\chi|\mathbf{F}_m|^2}{\psi^2\delta_t(\tau_c - 0.5)} \\ -6\mathbf{u} \cdot \mathbf{F} - \frac{12\chi|\mathbf{F}_m|^2}{\psi^2\delta_t(\tau_c - 0.5)} \\ F_x \\ -F_x \\ F_y \\ -F_y \\ 2(u_x F_x - u_y F_y) \\ (u_x F_y + u_y F_x) \end{bmatrix}, \quad (8)$$

where  $\chi$  can be adjusted to tune the mechanical stability condition. In this study,  $\chi$  is set to 0.1.  $\mathbf{F} = (F_x, F_y)$  is the total force, which contains the pseudopotential interaction force  $\mathbf{F}_m$ , the buoyancy force  $\mathbf{F}_b$ , and the solid–liquid interaction force  $\mathbf{F}_{ads}$ .  $\mathbf{F}_m$  is the basis of phase separation in the pseudopotential model, which is designed by mimicking the molecular interactions<sup>34,35</sup>

$$\mathbf{F}_m = -G\psi(\mathbf{x}) \sum_{\alpha} w_{\alpha}\psi(\mathbf{x} + \mathbf{e}_{\alpha})\mathbf{e}_{\alpha}, \quad (9)$$

where  $\Psi$  is the pseudopotential,  $G$  is the interaction strength, and  $w_{\alpha}$  is the weight coefficient. To represent the phase change of the fluid, the nonideal EOS can be introduced to the pseudopotential function via<sup>25</sup>

$$\psi = \sqrt{\frac{2[p_{EOS}(\rho, T) - \rho c_s^2]}{Gc^2}}. \quad (10)$$

In this work, the Peng–Robinson (P–R) EOS was chosen for its applicability to common fluids such as water and ammonia

$$p_{EOS} = \frac{\rho RT}{1 - b\rho} - \frac{a\phi(T)\rho^2}{1 + 2b\rho - b^2\rho^2}, \quad (11)$$

where

$$\phi(T) = \left[ 1 + (0.37464 + 1.54226\omega - 0.26992\omega^2) \left( 1 - \sqrt{T/T_c} \right) \right]^2, \quad (12)$$

$$a = 0.45724R^2T_c^2/p_c, \quad b = 0.0778RT_c/p_c. \quad (13)$$

The critical compressibility factor for the P–R EOS is

$$Z_c = \frac{p_c}{\rho_c RT_c} = 0.307, \quad (14)$$

where  $p_c$ ,  $T_c$ ,  $\rho_c$ , and  $\omega$  are the critical pressure, critical temperature, critical density, and the acentric factor of the working fluid, respectively.

Through a numerical test of one-dimensional liquid–vapor phase coexistence, it can be seen that the numerical results of the present model agree well with the solution of Maxwell construction as shown in Fig. 1. The maximum density ratio the present model achieved is 307 at  $T/T_c = 0.65$ .

To simulate the phase change heat transfer process, an energy equation solver is required to be coupled with the LB flow field solver.<sup>36</sup> Neglecting the viscous heat dissipation, the energy equation is given by

$$\rho T \frac{Ds}{Dt} = \nabla \cdot (\lambda \nabla T), \quad (15)$$

where  $s$  is the entropy,  $\lambda$  is the thermal conductivity, and  $\frac{D}{Dt}$  is the material derivative. Considering the thermodynamic relation  $ds = \frac{c_v}{T} dT + \left( \frac{\partial p_{EOS}}{\partial T} \right)_v dv$ , Eq. (15) is transformed to<sup>14</sup>

$$\frac{\partial T}{\partial t} = -\mathbf{u} \cdot \nabla T + \frac{1}{\rho c_v} \nabla \cdot (\lambda \nabla T) - \frac{T}{\rho c_v} \left( \frac{\partial p_{EOS}}{\partial T} \right)_\rho \nabla \cdot \mathbf{u}, \quad (16)$$

where  $c_v$  is the specific heat at constant volume. To solve Eq. (16), either the thermal LB solver or the FDM solver could be used. The latter approach is adopted in this paper, and the fourth-order Runge–Kutta scheme is used for time discretization. The detailed implementation can be found in Ref. 14.

### B. The conventional unit conversion method

In the previous pseudopotential LB boiling studies, the common method adopted for unit conversion is based on the combination of dimensionless parameter mapping and the principle of corresponding state,<sup>9,16–21</sup> which will be referred to as the conventional unit conversion method in Secs. III–V for simplicity. In pool boiling problems, the required group of dimensionless numbers determined from the Buckingham theorem is  $(Nu, Pr, Ja, L_H^*)$ ,<sup>16</sup> which are Nusselt number, Prandtl number, Jacob number, and dimensionless heater size, respectively. They are defined by

$$Nu = \frac{hL_H}{\lambda}, \quad Pr = \frac{\nu}{\alpha}, \quad Ja = \frac{c_p(T_w - T_s)}{h_{fg}}, \quad L_H^* = \frac{L_H}{l_0}, \quad (17)$$

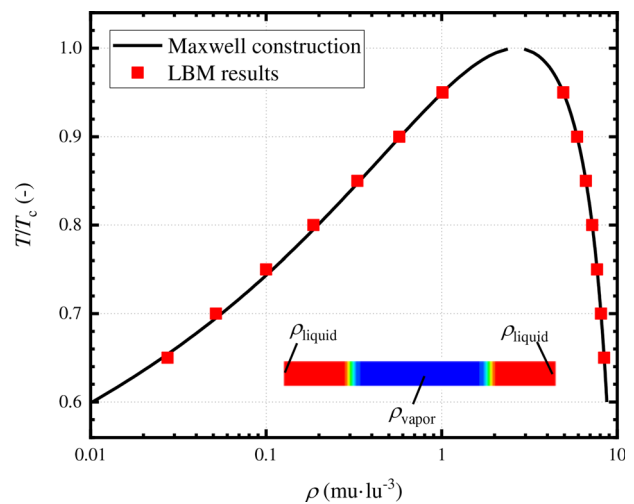


FIG. 1. Coexistence curve.

where  $L_H$  is the heater size;  $T_w$  and  $T_s$  are the wall temperature and saturated temperature, respectively; and  $h_{fg}$  is the specific latent heat which can be calculated from the EOS introduced with the pseudopotential function.<sup>37</sup>  $l_0$  is the characteristic length defined by the capillary length

$$l_0 = \sqrt{\frac{\sigma}{g(\rho_L - \rho_V)}}, \quad (18)$$

where  $\sigma$  is the surface tension and  $g$  is the gravitational acceleration. The value of  $\sigma$  can hardly be directly calculated in the pseudopotential model. It is usually numerically derived by stationary bubble test and Laplace law fitting.  $g$  is a self-defined parameter in the conventional method. With the definition of the characteristic length  $l_0$ , a reference velocity and a reference time can be determined accordingly by  $u_0 = \sqrt{gl_0}$ ,  $t_0 = l_0/u_0$ . Thus, the length and the time value in the LB simulations can be nondimensionalized by  $l^* = l/l_0$  and  $t^* = t/t_0$ .

Nondimensionalized results can be directly used for analyses and discussions, but the final results presented in physical units are often more concerned in practical engineering problems. Here, the procedure of the conventional unit conversion is illustrated in Fig. 2. Taking the conversion of an arbitrary length value as an example. A bubble's diameter in the LB simulation is known as  $D_{LS}$  in the unit of lu. The goal is to convert the diameter in lattice unit to the SI form  $D_{PS}$  in the unit of meter. It is specified that the subscript LS (lattice scale) indicates that the value is in lattice unit, whereas PS (physical scale) indicates that the value is in physical unit. First,  $\sigma_{LS}$ ,  $g_{LS}$ , and  $\Delta\rho_{LS}$  are determined in the LB system, and  $l_{0,LS}$  is calculated via Eq. (18). Second, the dimensionless diameter is calculated using  $D^* = D_{LS}/l_{0,LS}$ . Next,  $\sigma_{PS}$  and  $\Delta\rho_{PS}$  of the working fluid and the gravity  $g_{PS}$  are determined in physical units, and  $l_{0,PS}$  is also calculated using Eq. (18). Finally, by linking the lattice unit with physical unit through the dimensionless length, the real diameter in physical unit is derived using  $D_{PS} = D^*l_{0,PS}$ . Other quantities can also be converted to the physical unit form by a similar approach.

However, another set of unit scale for absolute temperature and pressure is implied in pseudopotential LB model, because the parameters in the nonideal EOS contain  $T_c$  and  $p_c$ , as in Eq. (13). According to the principle of corresponding state, the reduced temperature  $T_r = T/T_c$  and pressure  $p_r = p/p_c$  calculated in the lattice unit system should be equal to those in the physical unit system. Thus, the reduced values can be regarded as another bridge connecting the two unit

systems in addition to the mapping of the dimensionless number group. The reduced temperature  $T_r$  is widely used for the analyses in many previous studies on LB boiling simulations.<sup>9,16,18,19,21</sup> However, in the mapping of  $(Nu, Pr, Ja, L_H^*)$ , only the temperature difference ( $T_w - T_s$  in the definition of  $Ja$  number) and the pressure difference ( $\sigma = r\Delta p$  in the expression of  $l_0$ ) are linked, but there is no connection about the absolute temperature and pressure between the two unit systems. The critical values  $T_c$  and  $p_c$  and other related parameters in the EOS play no role in the connection of the two unit systems when mapping the dimensionless number group. This indicates that there may be inconsistency between the conversion method based on dimensionless number mapping and the method based on the principle of corresponding states, which will be demonstrated numerically in Sec. IV B.

### C. The novel approach of unit conversion

In this section, a novel unit conversion method based on the fundamental units is proposed for liquid–vapor phase change LB simulations. All physical quantities are composed of base quantities, whose units are referred to as fundamental units. For most heat transfer and fluid flow problems, M, L, T, and  $\Theta$  are the four related fundamental units, which correspond to mass  $m$ , length  $l$ , time  $t$ , and temperature  $T$ , respectively. If the lattice–physical unit conversion relations for all base quantities are known, the unit conversion relations for all physical quantities could be derived from these relations. The relations for the four base quantities are written as

$$\begin{aligned} m_{PS} &= m_r \cdot m_{LS}, & l_{PS} &= l_r \cdot l_{LS}, \\ t_{PS} &= t_r \cdot t_{LS}, & T_{PS} &= T_r \cdot T_{LS}, \end{aligned} \quad (19)$$

where the subscript r refers to “relation,” and the  $m_r$ ,  $l_r$ ,  $t_r$ , and  $T_r$  are the coefficients. The units of the four coefficients are kg/mu, m/lu, s/ts, and K/tu, respectively. For an arbitrary quantity  $\Phi$  with the dimension of  $\dim \Phi = M^{\alpha}L^{\beta}T^{\gamma}\Theta^{\delta}$ , the lattice–physical unit conversion relation is calculated by

$$\Phi_{PS} = \Phi_r \cdot \Phi_{LS}, \quad (20)$$

where

$$\Phi_r = m_r^{\alpha} l_r^{\beta} t_r^{\gamma} T_r^{\delta}. \quad (21)$$

In the case of the phase change LB model, the conversion relations of base quantities can be deduced from the fluid properties in the

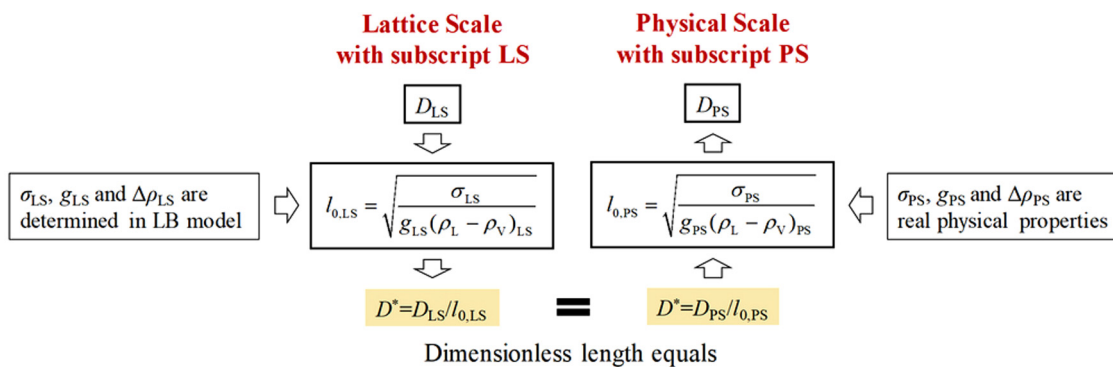


FIG. 2. Unit conversion of the bubble diameter using capillary length as the reference scale.

nonideal EOS introduced by the pseudopotential function. In this paper, the P-R EOS shown in Eq. (11) is taken as an example. On one hand, for a specific fluid, its specific gas constant,  $R_{PS}$ ; critical pressure,  $p_{c,PS}$ ; and critical temperature,  $T_{c,PS}$ , in the physical unit system are all known quantities. Then,  $a_{PS}$  and  $b_{PS}$  in the EOS in physical unit can be calculated using Eq. (13). On the other hand, the EOS parameters and the specific gas constant in the lattice unit system are specified in LB models before simulations. For example,  $a_{LS} = 3/49$ ,  $b_{LS} = 2/21$ , and  $R_{LS} = 1$  or other close values are often used, as shown in Table I. This indicates that  $a$ ,  $b$ , and  $R$  in both the physical unit system and the lattice unit system are determined and mutually matched, as long as the real fluid and the nonideal EOS in pseudopotential model are determined. Moreover, the surface tension  $\sigma_{PS}$  in physical unit is a known property at a specific saturated temperature  $T_s$ . In the pseudopotential LB model presented in Sec. II A,  $\sigma_{LS}$  is only affected by the saturated temperature, which means  $\sigma_{LS}$  is fixed and cannot be adjusted independently once the EOS parameters are determined. In summary, four parameters with independent units can be determined in both physical unit and lattice unit values when the fluid is specified and the nonideal EOS in the pseudopotential model is established.

For the P-R EOS, the lattice-physical unit conversion relations of the four parameters are given by

$$\begin{aligned} a_r &= \frac{a_{PS}}{a_{LS}}, & b_r &= \frac{b_{PS}}{b_{LS}}, \\ R_r &= \frac{R_{PS}}{R_{LS}}, & \sigma_r &= \frac{\sigma_{PS}}{\sigma_{LS}}. \end{aligned} \tag{22}$$

The dimensions of the four parameters are

$$\begin{aligned} \dim a &= M^{-1}L^5T^{-2}, \\ \dim b &= M^{-1}L^3, \\ \dim R &= L^2T^{-2}\Theta^{-1}, \\ \dim \sigma &= MT^{-2}. \end{aligned} \tag{23}$$

Substituting  $a$ ,  $b$ ,  $R$ , and  $\sigma$  into Eq. (21), the following relations can be derived:

$$\begin{aligned} a_r &= m_r^{-1}l_r^5t_r^{-2}, \\ b_r &= m_r^{-1}l_r^3, \\ R_r &= l_r^2t_r^{-2}T_r^{-1}, \\ \sigma_r &= m_rl_r^{-2}. \end{aligned} \tag{24}$$

The unit conversion relations of the four base quantities can then be solved as

$$\begin{aligned} m_r &= a_r^{-3}b_r^5\sigma_r^3, \\ l_r &= a_r^{-1}b_r^2\sigma_r, \\ t_r &= a_r^{-\frac{3}{2}}b_r^{\frac{5}{2}}\sigma_r, \\ T_r &= a_rl_r^{-1}R_r^{-1}. \end{aligned} \tag{25}$$

The lattice-physical unit conversion relations of all quantities can be derived using Eq. (20) with the established conversion relations of the base quantities  $m$ ,  $l$ ,  $t$ , and  $T$  via Eqs. (21) and (25). This implies that the units of macroscopic quantities (e.g., density, velocity) and the distribution function in the LB equation can all be converted using Eq. (25), which contains the EOS parameters  $a$ ,  $b$ , and  $R$ . Therefore, it is guaranteed that the units in the LB equation and units of the EOS parameters are consistent with each other. The procedure of the unit conversion based on the fundamental units is illustrated in Fig. 3.

Several remarks are made about the proposed unit conversion method:

- (i) According to Eqs. (13) and (14), the mapping of EOS parameters  $a$ ,  $b$ , and  $R$  is equivalent to the mapping of critical state parameters  $\rho_c$ ,  $p_c$  and  $T_c$ . For other nonideal EOSs that are often implemented in pseudopotential function, such as Redlich-Kwong EOS, Redlich-Kwong Soave EOS, and Carnahan-Starling EOS,<sup>25</sup> one can still choose to match the surface tension and  $\rho_c$ ,  $p_c$  and  $T_c$  to establish the four relations similar to Eq. (24).
- (ii) In the above analysis, there is no governing equation of any specific practical problems, so the method is not limited to pool boiling problems and can be applied to other kinds of pseudopotential LB liquid-vapor phase change simulations.
- (iii) Here, the length conversion coefficient  $l_r$  is an intrinsic value of the pseudopotential model and is only dependent on  $a_r$ ,  $b_r$ , and  $\sigma_r$  according to Eq. (25). The lattice gravity cannot be arbitrarily chosen and is determined by  $g_{LS} = g_{PS}/(l_r t_r^{-2})$ . However, in the conventional length conversion procedure, the coefficient is calculated by  $l_r = l_{0,PS}/l_{0,LS}$  according to Fig. 2, whereas  $l_{0,LS}$  depends on the pre-given value of  $g_{LS}$ . It can be seen that  $l_r$  calculated using the conventional method is distinct from the intrinsic  $l_r$  calculated using Eq. (25) if  $g_{LS}$  is an arbitrary value. Therefore, there will be a mismatch between the length scale when applying the conventional method, which will be demonstrated in Sec. IV B.

To be mentioned, the fundamental unit conversion factors ( $m_r$ ,  $l_r$ ,  $t_r$ ,  $T_r$ ) are related to the spatial and temporal resolutions in the LB simulation. In the present model, the adjustment of ( $m_r$ ,  $l_r$ ,  $t_r$ ,  $T_r$ )

Matching of surface tension + Matching of EOS parameters

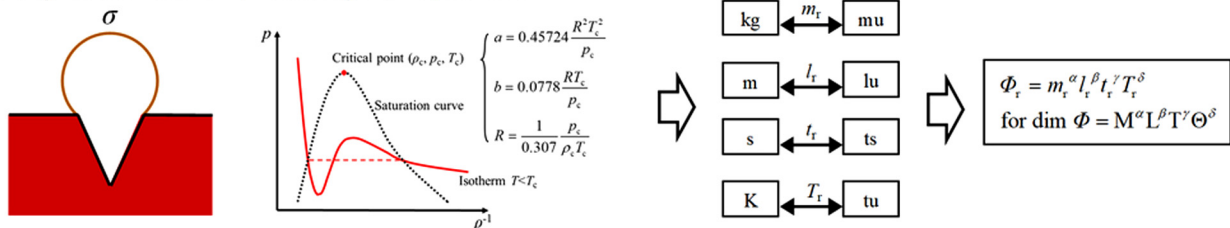


FIG. 3. Schematic representation of the proposed unit conversion process.

is determined by the tunability of  $(a, b, R, \sigma)_{LB}$ . The physical unit properties  $(a, b, R, \sigma)_{PS}$  are unchangeable once the fluid is selected. According to Table I, the lattice system EOS parameters  $b_{LS}$  and  $R_{LS}$  are always fixed, whereas  $a_{LS}$  is tunable, but the range is relatively limited. To improve the flexibility of the present model, it is necessary to introduce a scheme that can achieve a tunable surface tension  $\sigma_{LS}$  to adjust  $(m_r, l_r, t_r, T_r)$ . In this paper, the approach proposed by Li and Luo<sup>29</sup> is implemented, which adds a source term to the MRT collision equation to tune  $\sigma_{LS}$

$$\mathbf{m}^* = \mathbf{m} - \Lambda(\mathbf{m} - \mathbf{m}^{eq}) + \delta_t \left( \mathbf{I} - \frac{\Lambda}{2} \right) \mathbf{S} + \delta_t \mathbf{C}. \quad (26)$$

The source term  $\mathbf{C}$  is given by

$$\mathbf{C} = \begin{bmatrix} 0 \\ 1.5\tau_e^{-1}(Q_{xx} + Q_{yy}) \\ -1.5\tau_e^{-1}(Q_{xx} + Q_{yy}) \\ 0 \\ 0 \\ 0 \\ 0 \\ -\tau_\nu^{-1}(Q_{xx} - Q_{yy}) \\ -\tau_\nu^{-1}Q_{xy} \end{bmatrix}. \quad (27)$$

$\mathbf{Q}$  is calculated via

$$\mathbf{Q} = \kappa \frac{G}{2} \psi(\mathbf{x}) \sum_{\alpha=1}^8 w_\alpha [\psi(\mathbf{x} + \mathbf{e}_\alpha \delta_t) - \psi(\mathbf{x})] \mathbf{e}_\alpha \mathbf{e}_\alpha, \quad (28)$$

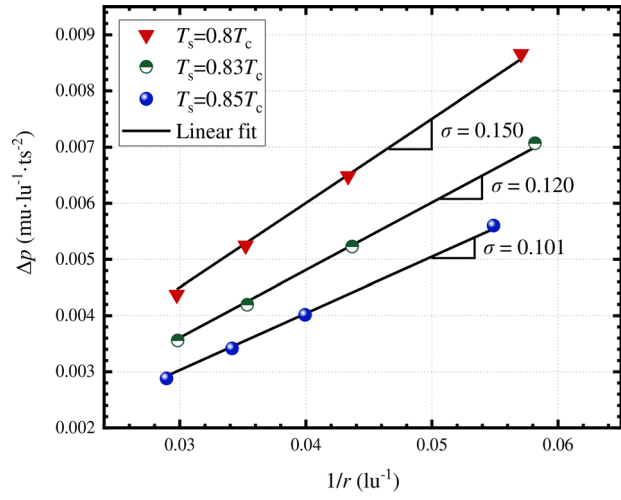
where the parameter  $\kappa$  is the coefficient for tuning the surface tension,  $\kappa \in (-1, 1)$ . Equation (26) will reduce to Eq. (3) when  $\kappa = 0$ . The adjustment of the fundamental unit conversion factors  $(m_r, l_r, t_r, T_r)$  can then be achieved by tuning  $\kappa$  to change  $\sigma_{LS}$ .

### III. MODEL VALIDATION

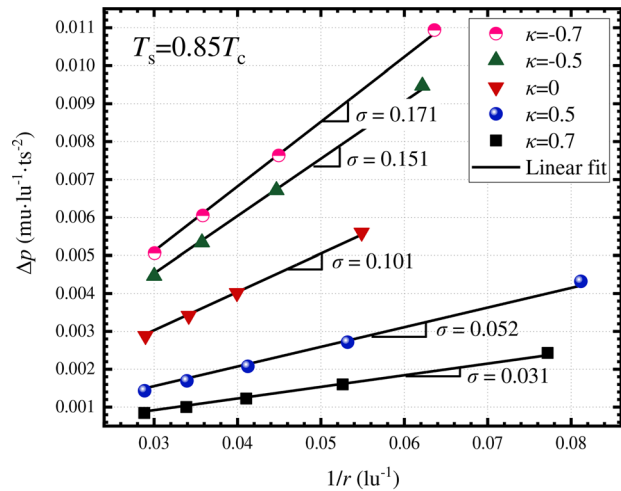
In this section, two benchmark problems are carried out to validate the hybrid thermal LB phase change model used in this work. The first problem is a stationary bubble test to evaluate the consistency with the Laplace law under an isothermal condition. The second is a droplet evaporation problem to validate the phase change heat transfer performance. The purpose of this section is to assess the validity of the simulation model in lattice scale, so that the results are all presented in lattice unit, and no unit conversion process is involved.

#### A. The Laplace law

For the first problem, round bubbles of different diameters are embedded in the center of a  $210 \times 210 \text{ lu}^2$  periodic simulation domain filled with liquid. The domain is set isothermal with no gravity. It is indicated in the 2D Laplace law  $\Delta p = \sigma/r$  that the pressure difference  $\Delta p$  across the bubble interface is proportional to the inverse of the radius  $1/r$ , and the slope is the surface tension  $\sigma$ . Figure 4(a) shows that there are good linear relationships between  $\Delta p$  and  $1/r$  at different saturated temperatures. The surface tension fitted at  $T_s = 0.8T_c$ ,  $0.83T_c$ , and  $0.85T_c$  is 0.150, 0.120, and 0.101, respectively. Figure 4(b) represents



(a)



(b)

FIG. 4. The result of the validation of Laplace law: (a)  $\kappa = 0$  at different saturated temperatures and (b)  $T_s = 0.85T_c$  with different  $\kappa$ .

the change in surface tension at a fixed saturated temperature, using the surface tension adjustment model given in Eq. (26). At  $T_s = 0.85T_c$ ,  $\sigma$  decreases from 0.171 to 0.031 with the change in  $\kappa$  from  $-0.7$  to  $0.7$ . The surface tension adjustment model is validated.

#### B. Droplet evaporation problem

For the second problem, the droplet evaporation heat transfer simulation is conducted to validate the thermal LB model with the energy equation solver.<sup>38–40</sup> A circular droplet is suspended in a finite 2D open system with a temperature boundary  $T_b = T_s + \Delta T$ . The system is gravity-free. Evaporation occurs on the droplet surface only due to diffusion. Assuming that the thermophysical properties ( $c_v, \lambda$ ) remain constant and the liquid and vapor are at a quasi-steady state,



an analytical solution of the droplet diameter  $D$  evolution in time  $t$  can be derived

$$\left[ \ln \left( \frac{L}{D} \right) + \frac{1}{2} \right] D^2 = \left[ \ln \left( \frac{L}{D_0} \right) + \frac{1}{2} \right] D_0^2 - Kt, \quad (29)$$

where  $K = \frac{8\lambda_V}{\rho_L c_{V,V}} \ln(1+B)$ ,  $B = \frac{c_{V,V}(T_b - T_s)}{h_{fg}}$ , and  $L$  is the size of the finite domain. A detailed derivation of Eq. (29) can be found in Ref. 39. A similar analytical solution can be derived for a spherical droplet evaporated in an infinite 3D domain, which is well known as the  $D^2$ -law.<sup>41</sup>

The 2D simulations in a  $L^2 = 200 \times 200$  lu<sup>2</sup> domain are implemented. Initially, a droplet with a diameter of  $D_0$  is suspended in the center of a domain filled with vapor. The temperature of the entire field is initialized at  $T_s = 0.85T_c$ . A Dirichlet temperature boundary of superheat temperature of  $0.1T_c$  is implemented to make the droplet evaporate under the temperature gradient. A non-equilibrium extrapolation scheme for constant pressure is used, which is consistent with the open system condition.<sup>42</sup> The pressure at the boundary is set to be the saturated pressure at  $T_s$ . The kinematic viscosity is set to be  $\nu = 0.137$  ( $\tau_\nu = 0.912$ ) in the whole simulation domain. The surface tension tuning coefficient  $\kappa$  is chosen to be 0.7. The latent heat  $h_{fg}$  is calculated from the EOS according to Ref. 37. Simulations with different parameters  $K=0.0117$ , 0.0038, and 0.0024 are conducted. The time evolution of  $D^2$  simulated by the LB model is presented in Fig. 5 by the scatter points, and the analytical solutions of Eq. (29) are presented by the solid lines. The numerical results agree well with the analytical curves. Therefore, the phase change heat transfer performance of the LB model is validated.

#### IV. RESULTS AND DISCUSSION

To validate the proposed unit conversion method based on the fundamental units, two simulations are carried out in this section. The first is a thin film evaporation problem, and the second is bubble nucleation and growth from a V-shaped cavity. Both of them are benchmark problems that are widely used for model validation in lattice unit,<sup>17,18,43–46</sup> but few studies have converted the results to

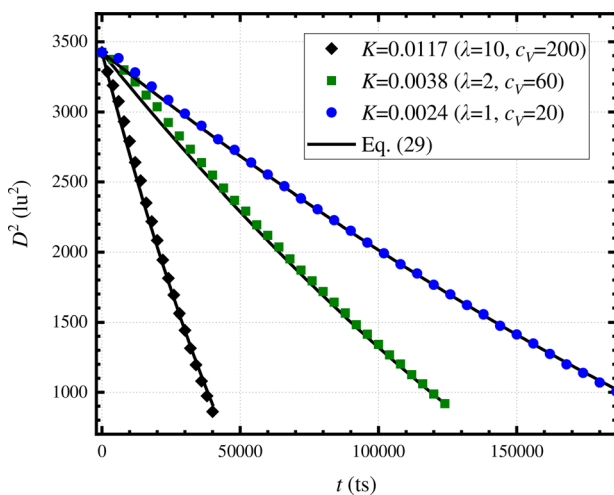


FIG. 5. The time evolution of  $D^2$  in droplet evaporation simulations.

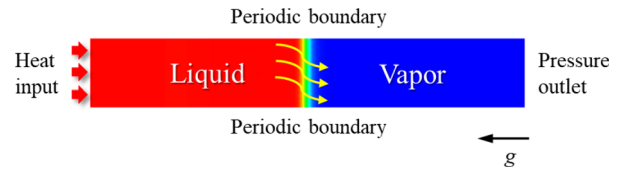


FIG. 6. Schematic representation of the computational domain of the thin film evaporation problem.

physical units and considered the actual properties of the working fluid. By simulating these problems and carrying out the unit conversion through the novel approach, the latent heat of the working fluid can be derived in physical unit, and the superheat temperature of the nucleation bubble is predicted. For comparison, in the second problem, the conventional unit conversion method will be implemented with the same pseudopotential model.

#### A. Derivation of specific latent heat from LB simulation

The thin film evaporation problem has been used for phase change heat transfer validation in pseudopotential LB studies by many researchers.<sup>43,44,47</sup> As shown in Fig. 6, the upper half of the domain is initialized as saturated vapor phase and the bottom is initialized as saturated liquid. The pressure outlet boundary is set on the right side,<sup>33</sup> and the constant heat flux is applied on the left-side wall. The top and bottom sides are periodic boundaries, so the domain can be regarded as a liquid film spread on an infinitely large heating surface. The heat flux on the wall is small enough that the vaporization occurs only at the surface of the film. Simulations are first conducted at  $T_s = 0.83T_c$  and  $q = 0.0001$  mu ts<sup>-3</sup> under different domain sizes. The lattice unit results of the stable steam mass flow rate  $m''$  are shown in Fig. 7. The computational domain size is thus chosen to be  $120 \times 20$  lu<sup>2</sup> for the consideration of accuracy and efficiency.

In the film evaporation problem, the relation of stable steam mass flow rate  $m''$  with heat flux  $q$  should satisfy

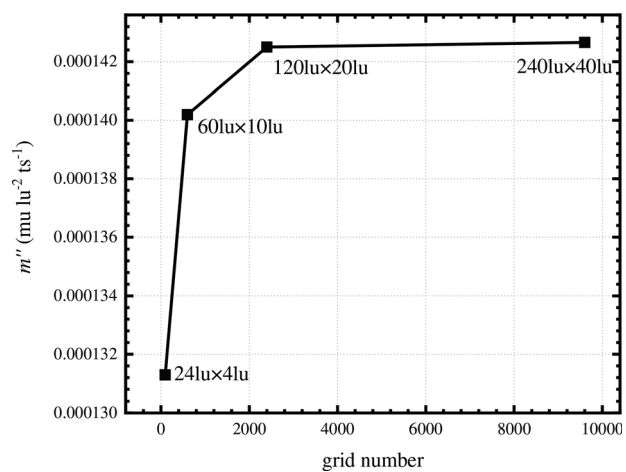


FIG. 7. Steam mass flow rate at  $T_s = 0.83T_c$  and  $q = 0.0001$  mu ts<sup>-3</sup>, simulated under different domain sizes.

**TABLE II.** Lattice–physical unit conversion based on the fundamental unit.

	Case 1	Case 2
$a_{LS}$ ( $\text{mu}^{-1} \text{lu}^5 \text{ts}^{-2}$ )	3/49	3/49
$a_{PS}$ ( $\text{kg}^{-1} \text{m}^5 \text{s}^{-2}$ )	1848.1	1848.1
$b_{LS}$ ( $\text{mu}^{-1} \text{lu}^3$ )	2/21	2/21
$b_{PS}$ ( $\text{kg}^{-1} \text{m}^3$ )	0.0011	0.0011
$R_{LS}$ ( $\text{lu}^2 \text{ts}^{-2} \text{tu}^{-1}$ )	1	1
$R_{PS}$ ( $\text{J kg}^{-1}$ )	461.5	461.5
$\sigma_{LS}$ ( $\text{mu ts}^{-2}$ )	0.1203	0.0308
$\sigma_{PS}$ ( $\text{kg s}^{-2}$ )	0.0228	0.0197
$m_r$ ( $\text{kg/mu}$ )	$4.07 \times 10^{-26}$	$1.58 \times 10^{-24}$
$l_r$ ( $\text{m/lu}$ )	$7.66 \times 10^{-10}$	$2.59 \times 10^{-9}$
$t_r$ ( $\text{s/ts}$ )	$4.64 \times 10^{-13}$	$1.57 \times 10^{-12}$
$T_r$ ( $\text{K/tu}$ )	$5.916 \times 10^3$	$5.916 \times 10^3$

$$q = h_{fg} m'' \tag{30}$$

where  $h_{fg}$  is the specific latent heat of the working fluid. An analytical method to determine the value of  $h_{fg}$  via EOS has been proposed in Ref. 37. In many previous studies, this method has been implemented to calculate  $h_{fg}$  in the lattice unit system as a standard to validate the simulation results of the thin film evaporation problem in lattice units.<sup>20,48</sup> In this section, the original LB results are converted to physical units directly using the novel conversion method and are compared with the fluid’s actual latent heat.

Two cases are simulated. For case 1, the saturated temperature is initialized as  $0.83T_c$ , and the surface tension tuning coefficient  $\kappa$  is taken as 0, whereas for case 2, the saturated temperature is initialized as  $0.85T_c$ , and  $\kappa$  is set to 0.7. Water is chosen as the working fluid, and the EOS parameters in the lattice unit system are  $a_{LS} = 3/49$ ,  $b_{LS} = 2/21$ , and  $R_{LS} = 1$ , and the acentric factor for water is  $\omega = 0.344$ . The EOS parameters  $a_{PS}$  and  $b_{PS}$  in the physical unit system are given by the critical properties of water, and the real surface tension  $\sigma_{PS}$  is derived from NIST WebBook database.<sup>49</sup> The surface

tension in lattice unit is taken from the fitting results in Sec. III A, which are 0.1203 and 0.0308 for cases 1 and 2, respectively. The lattice–physical unit conversion relations of the four base quantities can then be calculated via Eqs. (22) and (25). Table II gives the corresponding values of  $a$ ,  $b$ ,  $R$ , and  $\sigma$  and the conversion coefficients of the base quantities, from which the unit conversion relations of any arbitrary quantities can be derived according to Eq. (20). In particular, the input parameters of the LB model such as water thermodynamic properties are determined by converting the NIST values from physical units to lattice units. The specific parameters and the converted results are shown in Table III. The phase equilibrium densities in pseudopotential LB liquid–vapor coexistence simulations deviate from those converted from NIST values by 26% for liquid density and 8% for vapor density. This is caused by the deviation of the P–R EOS from the actual physical properties. The initialized densities in the simulation are chosen as the LB equilibrium densities (values in parentheses in Table III).

Different steam mass flow rates  $m''$  can be simulated by changing the heat flux  $q$  applied on the bottom wall, as shown in Fig. 8. It is indicated that  $m''$  varies proportionally with  $q$ . The top and right axes are  $m''$  and  $q$  represented in physical units transferred by the fundamental unit conversion relations in Table II. The specific latent heat of water  $h_{fg}$  can then be derived by a linear fit of the LB simulation results via Eq. (30). The physical unit  $h_{fg}$  obtained from case 1 is 1729.45 kJ/kg, whereas the value in NIST database is 1639.60 kJ/kg at  $T_s = 0.83T_c = 537.1 \text{ K}$ , leading to a relative deviation of 5.5%. As to  $T_s = 0.85T_c = 550.0 \text{ K}$  in case 2, the NIST database gives an  $h_{fg}$  of 1562.63 kJ/kg, whereas the simulation result comes out as 1609.54 kJ/kg, deviating by 3.0%. The deviation is caused by the difference between the P–R EOS and the actual fluid properties. A relation between the latent heat and the EOS has been proposed in Appendix A of Ref. 37

$$h_{fg} = h_V - h_L = - \int_L^V \frac{1}{\rho^2} \left[ T \left( \frac{\partial p}{\partial T} \right)_\rho - p \right] d\rho + \left( \frac{p}{\rho} \right) \Big|_L^V \tag{31}$$

It is indicated that latent heat can be regarded as a derived property from EOS; thus, the accuracy of unit conversion of EOS guarantees that the latent heat in phase change LB simulation is consistent with

**TABLE III.** Physical–lattice unit conversion of input parameters. The density values in parentheses account for the equilibrium density in the pseudopotential LB model, and the values outside account for the lattice unit density converted from the NIST value.

Parameters	Case 1		Case 2	
	In physical units	In lattice unit	In physical units	In lattice unit
Liquid specific heat capacity at constant volume, $c_{V,L}$	3.12 kJ kg <sup>-1</sup> K <sup>-1</sup>	6.76 lu <sup>2</sup> ts <sup>-2</sup> tu <sup>-1</sup>	3.09 kJ kg <sup>-1</sup> K <sup>-1</sup>	6.70 lu <sup>2</sup> ts <sup>-2</sup> tu <sup>-1</sup>
Vapor specific heat capacity at constant volume, $c_{V,V}$	2.59 kJ kg <sup>-1</sup> K <sup>-1</sup>	5.62 lu <sup>2</sup> ts <sup>-2</sup> tu <sup>-1</sup>	2.72 kJ kg <sup>-1</sup> K <sup>-1</sup>	5.89 lu <sup>2</sup> ts <sup>-2</sup> tu <sup>-1</sup>
Liquid heat conductivity, $\lambda_L$	0.604 W m <sup>-1</sup> K <sup>-1</sup>	11.43 mu lu ts <sup>-3</sup> tu <sup>-1</sup>	0.586 W m <sup>-1</sup> K <sup>-1</sup>	3.28 mu lu ts <sup>-3</sup> tu <sup>-1</sup>
Vapor heat conductivity, $\lambda_V$	0.055 W m <sup>-1</sup> K <sup>-1</sup>	1.04 mu lu ts <sup>-3</sup> tu <sup>-1</sup>	0.060 W m <sup>-1</sup> K <sup>-1</sup>	0.33 mu lu ts <sup>-3</sup> tu <sup>-1</sup>
Liquid kinematic viscosity, $\nu_L$	$1.29 \times 10^{-7} \text{ m}^2 \text{ s}^{-1}$	0.102 lu <sup>2</sup> ts <sup>-1</sup>	$1.25 \times 10^{-7} \text{ m}^2 \text{ s}^{-1}$	0.029 lu <sup>2</sup> ts <sup>-1</sup>
Vapor kinematic viscosity, $\nu_V$	$7.08 \times 10^{-7} \text{ m}^2 \text{ s}^{-1}$	0.560 lu <sup>2</sup> ts <sup>-1</sup>	$5.87 \times 10^{-7} \text{ m}^2 \text{ s}^{-1}$	0.137 lu <sup>2</sup> ts <sup>-1</sup>
Liquid density, $\rho_L$	777.37 kg m <sup>-3</sup>	8.60 (6.87) mu lu <sup>-3</sup>	755.75 kg m <sup>-3</sup>	8.36 (6.63) mu lu <sup>-3</sup>
Vapor density, $\rho_V$	25.35 kg m <sup>-3</sup>	0.28 (0.26) mu lu <sup>-3</sup>	31.49 kg m <sup>-3</sup>	0.35 (0.33) mu lu <sup>-3</sup>
Gravity, $g$	9.8 m s <sup>-2</sup>	$2.75 \times 10^{-15} \text{ lu ts}^{-2}$	9.8 m s <sup>-2</sup>	$9.31 \times 10^{-15} \text{ lu ts}^{-2}$

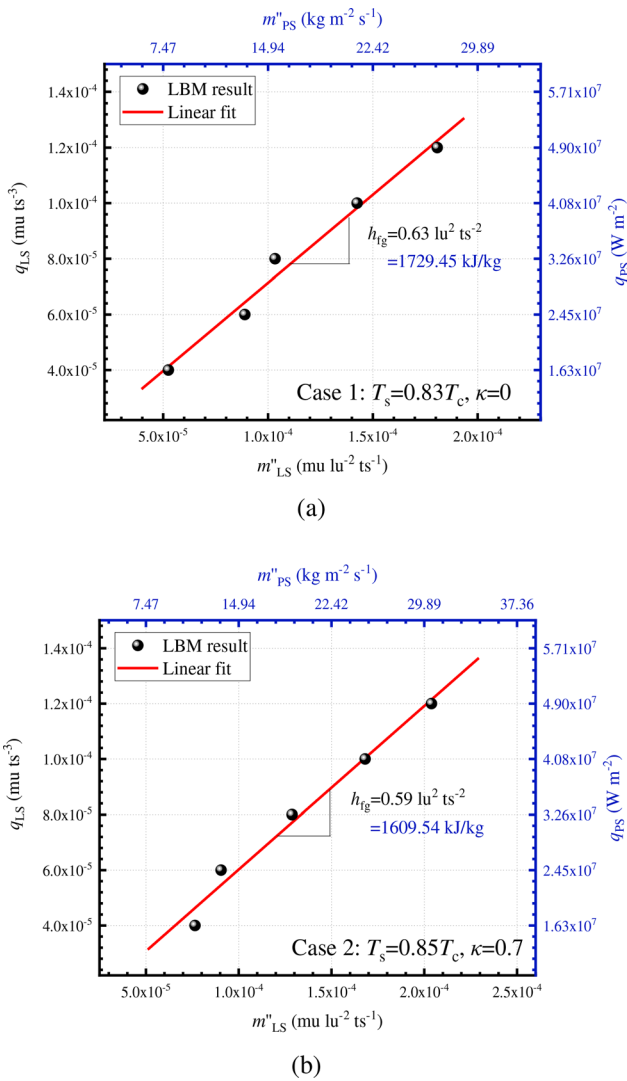


FIG. 8. Results of the thin film evaporation in lattice units and physical units: (a) case 1:  $T_s = 0.83T_c$ ,  $\kappa = 0$  and (b) case 2:  $T_s = 0.85T_c$ ,  $\kappa = 0.7$ .

the actual fluid property. In the novel unit conversion method proposed in this paper, the conversion relations of base quantities are solved according to the mapping relations of EOS parameters  $a$ ,  $b$ , and  $R$  from lattice unit to physical unit. The conversion relations of the four base quantities are established based on the relations between the lattice unit EOS  $p_{LS} = p_{EOS}(\rho_{LS}, T_{LS}, a_{LS}, b_{LS}, R_{LS})$  and the physical unit EOS  $p_{PS} = p_{EOS}(\rho_{PS}, T_{PS}, a_{PS}, b_{PS}, R_{PS})$ . This could explain why the physical unit latent heat derived from thin film evaporation LB simulation by the novel unit conversion method is basically consistent with the actual physical property.

### B. Bubble heterogeneous nucleation from a V-shaped cavity

Predicting the wall superheat temperature accurately is one of the key issues of LB boiling simulation. In recent years, the simulation of

bubble nucleation and growth from a V-shaped cavity has been applied by some researchers as a benchmark problem to validate the critical nucleation superheat.<sup>18,45,46</sup> The computational domain is a  $300 \times 400 \text{ lu}^2$  rectangle. As Fig. 9 illustrates, a solid wall with thickness of  $H = 140 \text{ lu}$  is located at the bottom of the domain with a V-shaped cavity. The vertical depth of the cavity is  $H_d = 130 \text{ lu}$ . The angle  $\gamma$  determines the mouth width of the cavity. Pressure outlet boundary is specified at the top,<sup>33</sup> and constant superheat temperature is applied at the bottom. Periodic boundaries are set to the left and right sides. The modified Mei-Luo-Shy curve boundary is employed at the fluid-solid interface to eliminate the effect of step approximation on liquid-vapor phase change,<sup>50,51</sup> and the contact angle is set to  $90^\circ$ . The initial temperature of the entire domain is set to  $T_s$ . The fluid domain inside the cavity is initialized as saturated vapor, whereas the other is initialized as saturated liquid. To reach an equilibrium start state, the simulation is run isothermally between  $0 \leq t \leq 5000 \text{ ts}$ . Then, after  $t > 5000 \text{ ts}$ , the energy equation solver is activated, and the wall superheat is applied.

Figure 10 shows the bubble heterogeneous growing process. Under the effect of bottom wall superheat, the vapor in the cavity begins to expand, and the liquid-vapor phase interface rises gradually. When the phase interface reaches the mouth of the cavity, the three-phase contact line will be pinned temporarily at the mouth, as shown by the bubble contours of  $t = 40\,000 - 70\,000 \text{ ts}$  in Fig. 10(a). At this stage, the curvature radius decreases with the increase in bubble volume [as shown by line AB in Fig. 10(b)] until the radius reaches its minimum at  $t = 130\,000 \text{ ts}$ , which is defined as the critical radius  $r_{cr}$ . Afterward, if the bubble continues to grow, the contact line will break the pinning effect and spread outward on the solid substrate, as shown by the bubble contours of  $t = 330\,000 - 350\,000 \text{ ts}$ , and the bubble radius increases consequently. Considering the Clausius-Clapeyron equation with the Laplace law describing surface tension, the relation between the critical superheat of the liquid film and the bubble critical radius is given as<sup>52</sup>

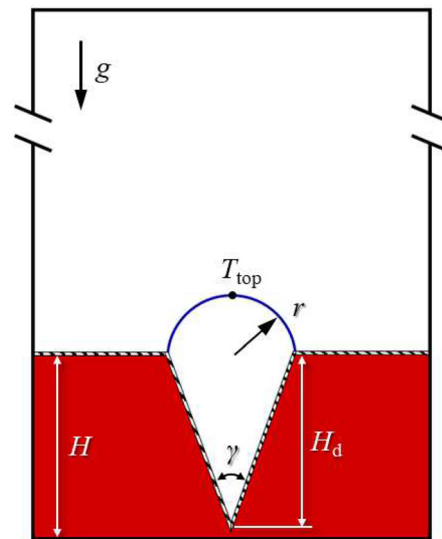


FIG. 9. Schematic representation of the V-shaped cavity computational domain.

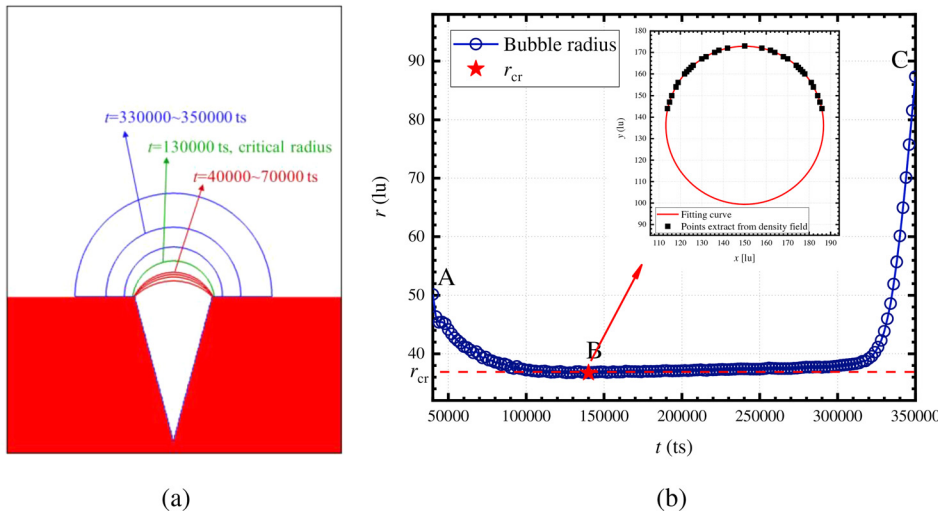


FIG. 10. Bubble heterogeneous nucleation process in a V-shaped cavity with  $\gamma = 30^\circ$ : (a) the shape of the bubble, (b) the radius of curvature of the bubble vs time and the fitting of a bubble contour (the interpolated figure).

$$\Delta T_s = \frac{\sigma T_s}{h_{fg} \rho_V r_{cr}}, \quad (32)$$

where  $\Delta T_s = T_{top} - T_s$ ,  $T_{top}$  is taken as the liquid temperature near the top of the bubble as pointed in Fig. 9. Equation (32) describes the thermodynamic condition of the bubble heterogeneous nucleation. The maximum superheat temperature  $\Delta T_s$  for the bubble to break the constrain of the surface tension corresponds to the maximum radius  $r_{cr}$  during the bubble growing process. The superheat temperature of the heating liquid near the bubble must be higher than  $\Delta T_s$  for the bubble to continue to expand. Otherwise, it will cease growing.

To verify the accuracy of the model with the novel unit conversion method in predicting superheat temperature in the physical unit system, bubble nucleation simulations in cavity with  $\gamma = 30^\circ, 40^\circ, 50^\circ$ , and  $60^\circ$  at saturated temperature  $T_s = 0.80T_c, 0.83T_c$ , and  $0.90T_c$  are carried out, respectively. For a specific cavity shape, the acquirement of  $\Delta T_s$  needs appropriate adjustment of wall temperature  $T_b$  to maintain a quasi-steady state in which the bubble can reach  $r_{cr}$  as close as possible without further expansion. In this paper, the squeezing strategy described in Ref. 18 is employed to control  $T_b$ . The simulations take water as the working fluid and initiate at the saturated temperature. The EOS parameters  $a, b$ , and  $R$  and surface tension tuning coefficient  $\kappa$  are set as same as case 1 in Sec. IV A, except that the kinematic viscosity of vapor is set as same as liquid  $\nu_V = \nu_L$  for the concern of model stableness. The approximation of no macroscopic flow in the fluid domain could be made for the quasi-steady state of bubble growing, thus the effect of the deviation of vapor kinematic

viscosity on heat transfer can be ignored. The solid properties are given by  $\rho_{solid} = 3\rho_L$  and  $\lambda_{solid} = 10\lambda_L$ . The conversion coefficients of base quantities derived by the novel unit conversion method are presented in Table IV. The physical unit result converted according to the fundamental unit relationship is shown in Fig. 11. The solid curves in Fig. 11 represent the analytical results given in Eq. (32). The physical properties  $\sigma, h_{fg}$ , and  $\rho_V$  in the equation are taken as NIST values. It is needed to be mentioned that  $\sigma$  is chosen at the temperature of  $T_{top} = T_s + \Delta T_s$  considering the influence of temperature variations on surface tension. It can be seen in Fig. 11 that the simulated superheat in the physical unit form recovered by the novel unit conversion method is basically consistent with the analytical result. It is proved previously in Sec. IV A that the actual latent heat and equilibrium density can be derived by LB phase change model with the novel unit

TABLE IV. Fundamental unit conversion relations of cases at different saturated temperatures derived by the novel unit conversion method.

	$T_s = 0.80T_c$	$T_s = 0.83T_c$	$T_s = 0.90T_c$
$m_r$ (kg/mu)	$3.62 \times 10^{-26}$	$4.07 \times 10^{-26}$	$5.74 \times 10^{-26}$
$l_r$ (m/lu)	$7.37 \times 10^{-10}$	$7.66 \times 10^{-10}$	$8.59 \times 10^{-10}$
$t_r$ (s/ts)	$4.46 \times 10^{-13}$	$4.64 \times 10^{-13}$	$5.20 \times 10^{-13}$
$T_r$ (K/tu)	$5.916 \times 10^3$	$5.916 \times 10^3$	$5.916 \times 10^3$

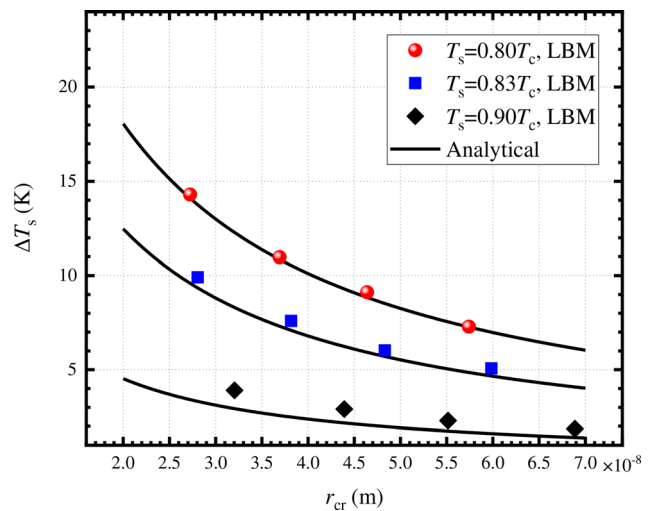


FIG. 11. The physical unit results of the bubble nucleation critical overheat temperature recovered by the novel unit conversion method based on the fundamental units.

**TABLE V.** Conventional unit conversion set 1 at different saturated temperatures with spatial resolution of  $10^{-6}$  m/lu.

		$\sigma$ (mu/ts <sup>2</sup> , kg/s <sup>2</sup> )	$\rho_L$ (mu/lu <sup>3</sup> , kg/m <sup>3</sup> )	$\rho_V$ (mu/lu <sup>3</sup> , kg/m <sup>3</sup> )	$g$ (lu/ts <sup>2</sup> , m/s <sup>2</sup> )	$l_0$ (lu, m)	$T_c$ (tu, K)
$T_s = 0.80T_c$	Lattice unit	0.1501	7.20	0.18	$6.05 \times 10^{-7}$	188.03	0.109 38
	Physical unit	0.0273	806.91	18.14	9.8	$1.8803 \times 10^{-3}$	647.10
$T_s = 0.83T_c$	Lattice unit	0.1203	6.87	0.26	$5.89 \times 10^{-7}$	175.74	0.109 38
	Physical unit	0.0228	777.37	25.35	9.8	$1.7574 \times 10^{-3}$	647.10
$T_s = 0.90T_c$	Lattice unit	0.0578	5.90	0.57	$5.53 \times 10^{-7}$	139.98	0.109 38
	Physical unit	0.0123	692.38	53.85	9.8	$1.3998 \times 10^{-3}$	647.10

conversion method, which are approximately consistent with the NIST value, whereas the correspondence of  $\sigma_{LS}$  and  $\sigma_{PS}$  is one of the constraints to establish the conversion relations of base quantities in Eq. (25). As a consequence, it is reasonable that the superheat temperature calculated in this approach agrees with the analytical result of Eq. (32). As  $T_s$  gets closer to the critical temperature, the case  $T_s = 0.90T_c$  shows deviation from the analytical solution Eq. (32). This is expected since Eq. (32) is derived under the assumption of a uniform-temperature liquid.<sup>53</sup> However, in the simulation, the liquid is heated by the solid wall and is non-isothermal. In this case, the superheat temperature required for bubble formation will be larger than what Eq. (32) predicts.<sup>53</sup> As  $T_s$  is closer to the critical temperature, fluid properties such as  $\rho$  and  $h_{fg}$  are more significantly affected by temperature variations. This could explain the deviation of case  $T_s = 0.90T_c$ .

For comparison, the conventional unit conversion method is employed to determine the LB input parameters and to recover the physical units in a bubble nucleation simulation. The lattice unit properties for a two-phase liquid are set to satisfy that the Prandtl number obtained from lattice unit values is consistent with the actual physical properties. Two sets of simulations are carried out. For set 1, simulations are carried out at different saturated temperatures  $T_s = 0.80T_c$ ,  $0.83T_c$ , and  $0.90T_c$ , whereas the spatial resolution of the lattice is fixed at  $10^{-5}$  m/lu. The corresponding lattice gravity for each saturated temperature is calculated via Eq. (18). The parameters are shown in Table V. For set 2, the saturated temperature is fixed at  $T_s = 0.80T_c$ , whereas the gravity is tuned according to Eq. (18) to achieve spatial resolutions of  $l_r = 10^{-5}$ ,  $10^{-6}$ , and  $10^{-7}$  m/lu, respectively. The corresponding parameters are listed in Table VI. For both sets, the critical temperatures in lattice unit and physical unit are  $T_{c,LS} = 0.109 38$  tu and  $T_{c,PS} = 647.10$  K,

respectively, leading to a temperature conversion relation of 5915.87 K/tu. The physical unit results converted by the above relations are plotted in Fig. 12, whereas the analytical line is still given by Eq. (32) with the parameters of NIST values. It can be seen that the simulation results recovered to physical units using the conventional method is several orders of magnitude larger than the analytical value. This is caused by the arbitrary lattice gravity  $g_{LS}$  and the improper calculation of the length conversion coefficient  $l_r$  by capillary length, as discussed in remark (iii) in Sec. II C. As shown in Fig. 12(b), when  $l_r$  is smaller (which means smaller lattice gravity and is closer to the  $l_r$  in Table IV), the converted LB simulation result gets closer to the analytical curve. It can be inferred that the simulation results could be in agreement with the analytical curve only if  $l_r$  is set to be the value calculated by the novel unit conversion method (i.e.,  $l_r = 7.37 \times 10^{-10}$  m/lu given in Table IV).

The inconsistency of the unit scale in the conventional conversion method can be further inferred. In the EOS expression in Eq. (11), the temperature and pressure are taken as absolute values, as well as in the analytical calculation of latent heat expression [Eq. (31)] and critical nucleation superheat [Eq. (32)]. However, in the unit conversion process based on the correspondence of dimensionless number group ( $Nu, Pr, Ja, l^*$ ), only the temperature difference [shown by  $(T_w - T_s)$  in the definition of  $Ja$ ] and pressure difference (shown by  $\sigma = r\Delta p$  in the definition of characteristic length  $l_0$ ) are connected between the lattice unit system and the physical unit system. There is no link between the absolute temperature and pressure. Figure 12 indicated that there is an inconsistency between the unit conversion scale defined by the correspondence of the dimensionless number group ( $Nu, Pr, Ja, l^*$ ) and the unit conversion scale of absolute temperature

**TABLE VI.** Conventional unit conversion set 2 with different spatial resolutions at  $T_s = 0.80T_c$ .

		$g$ (lu/ts <sup>2</sup> , m/s <sup>2</sup> )	$l_0$ (lu, m)	Other parameters
$l_r = 10^{-5}$ m/lu	Lattice unit	$6.05 \times 10^{-7}$	188.03	$\sigma_{LS} = 0.1501$ mu/ts <sup>2</sup> , $\sigma_{PS} = 0.0273$ kg/s <sup>2</sup> ; $\rho_{L,LS} = 7.20$ mu/lu <sup>3</sup> , $\rho_{L,PS} = 806.91$ kg/m <sup>3</sup> ; $\rho_{V,LS} = 0.18$ mu/lu <sup>3</sup> , $\rho_{V,PS} = 18.14$ kg/m <sup>3</sup> ; $T_{c,LS} = 0.109 38$ tu, $T_{c,PS} = 647.10$ K.
	Physical unit	9.8	$1.8803 \times 10^{-3}$	
$l_r = 10^{-6}$ m/lu	Lattice unit	$6.05 \times 10^{-9}$	$1.8803 \times 10^3$	
	Physical unit	9.8	$1.8803 \times 10^{-3}$	
$l_r = 10^{-7}$ m/lu	Lattice unit	$6.05 \times 10^{-11}$	$1.8803 \times 10^4$	
	Physical unit	9.8	$1.8803 \times 10^{-3}$	

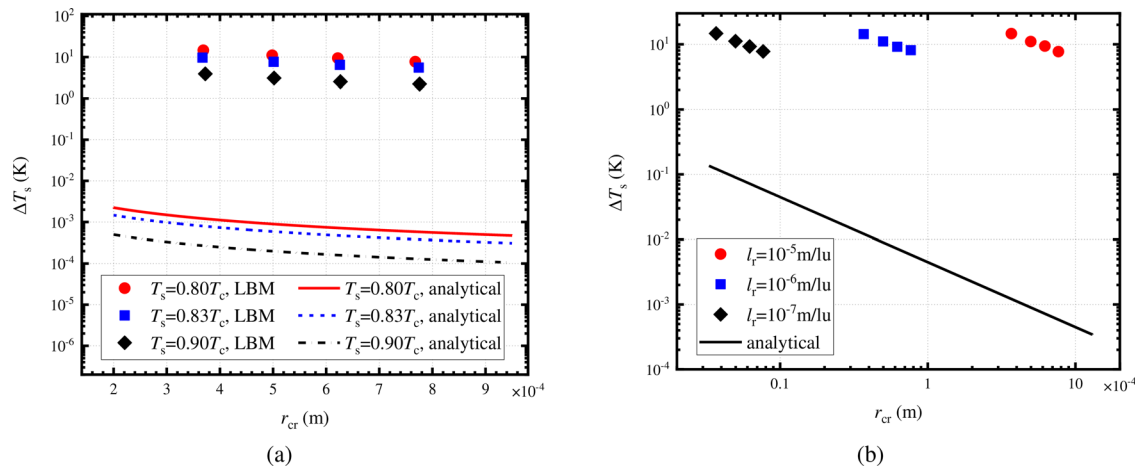


**FIG. 12.** The physical unit results of the bubble nucleation critical overheating temperature recovered by the conventional unit conversion method: (a) set 1:  $T_s$  is changed, and spatial resolution is fixed at  $10^{-6}$  m/lu, (b) set 2: spatial resolution is  $l_r$  changed, and the saturated temperature is fixed at  $T_s = 0.80T_c$ .

and pressure determined by the principle of corresponding state in EOS. Therefore, the conventional unit conversion method has a problem in calculating physical unit superheat temperature  $\Delta T_s$  in bubble nucleation processes.

**V. CONCLUSIONS**

A novel lattice–physical unit conversion method based on the fundamental unit is proposed for pseudopotential LB simulations for liquid–vapor phase change heat transfer. In the proposed method, the unit conversion relations of the base quantities are obtained from the correspondence of the EOS parameters  $a$ ,  $b$ , and  $R$  and the surface tension  $\sigma$ , and thus, the unit conversion relations of any other physical quantities can be derived by the combination of the fundamental unit conversion relations. The film evaporation problem is conducted, and it is proved that the proposed method enables the simulation result to recover the correct latent heat of fluid in physical unit. For the bubble nucleation and growth from a V-shaped cavity, the critical superheat temperature is accurately predicted in physical unit as a function of critical radius using the proposed unit conversion method. Comparatively, the superheat temperature recovered by the conventional unit conversion method based on dimensionless quantities correspondence and the principle of corresponding state has a deviation of orders of magnitude from the analytical value. This work aims to demonstrate the importance of a complete unit conversion method for the results of pseudopotential LB simulations for vapor–liquid phase change heat transfer. Further studies can be conducted on the range of spatial and time scales that can be simulated based on the proposed method and its extension.

**ACKNOWLEDGMENTS**

This work was supported by the National Natural Science Foundation of China (Nos. 51888103, 51721004, and 51906186).

**AUTHOR DECLARATIONS**

**Conflict of Interest**

The authors have no conflicts to disclose.

**Author Contributions**

**Si-Cheng Wang:** Formal analysis (equal); Investigation (equal); Methodology (equal); Software (equal); Validation (equal); Writing—original draft (lead). **Zi-Xiang Tong:** Conceptualization (equal); Formal analysis (equal); Methodology (equal); Supervision (equal); Writing—review and editing (equal). **Ya-Ling He:** Conceptualization (equal); Funding acquisition (equal); Methodology (equal); Project administration (equal); Supervision (equal); Writing—review and editing (equal). **Xiang Liu:** Formal analysis (equal); Methodology (equal).

**DATA AVAILABILITY**

The data that support the findings of this study are available from the corresponding author upon reasonable request.

**NOMENCLATURE**

- $a, b$  parameter in P–R equation of state
- $c$  lattice speed
- $c_V$  specific heat capacity at constant volume
- $e_x$  lattice velocity vector of  $x$  direction
- $f_x$  density distribution function
- $\mathbf{F}$  body force vector
- $g$  gravitational acceleration
- $h_{ig}$  specific latent heat
- $H_d$  the depth of the cavity
- $Ja$  Jacob number  $Ja = \frac{c_p(T_w - T_s)}{h_{ig}}$
- $l$  length
- $m$  mass
- $\mathbf{m}$  moment of density distribution function
- $Nu$  Nusselt number  $Nu = \frac{h_l}{\lambda}$
- $p$  pressure
- $Pr$  Prandtl number  $Pr = \frac{\nu}{\alpha}$
- $q$  heat flux
- $r_{cr}$  bubble critical radius
- $t$  time

$T$  temperature  
 $\Delta T_s$  bubble overheat temperature

### Greek symbol

$\alpha$  thermal diffusivity  
 $\lambda$  thermal conductivity  
 $\hat{\Lambda}$  MRT collision matrix  
 $\mu$  dynamic viscosity  
 $\nu$  kinematic viscosity  
 $\rho$  density  
 $\sigma$  surface tension  
 $\tau$  relaxation time  
 $\psi$  pseudopotential  
 $\omega$  acentric factor

### Subscripts

c critical  
 L liquid  
 LS lattice system  
 PS physical system  
 r relation  
 R reduced  
 s saturation  
 V vapor  
 0 characteristic  
 $\alpha$  lattice direction

### Superscripts

eq equilibrium  
 \* dimensionless quantities  
 ' post-collision quantities

### REFERENCES

- <sup>1</sup>J. W. Palko, H. Lee, C. Zhang, T. J. Dusseault, T. Maitra, Y. Won, D. D. Agonafer, J. Moss, F. Houshmand, G. Rong, J. D. Wilbur, D. Rockosi, I. Mykita, D. Resler, D. Altman, M. Asheghi, J. G. Santiago, and K. E. Goodson, "Extreme two-phase cooling from laser-etched diamond and conformal, template-fabricated microporous copper," *Adv. Funct. Mater.* **27**, 1703265 (2017).
- <sup>2</sup>R. Wen, Q. Li, W. Wang, B. Latour, C. H. Li, C. Li, Y. C. Lee, and R. Yang, "Enhanced bubble nucleation and liquid rewetting for highly efficient boiling heat transfer on two-level hierarchical surfaces with patterned copper nanowire arrays," *Nano Energy* **38**, 59 (2017).
- <sup>3</sup>T. G. Karayiannis and M. M. Mahmoud, "Flow boiling in microchannels: Fundamentals and applications," *Appl. Therm. Eng.* **115**, 1372 (2017).
- <sup>4</sup>H. Cao, Q. Zuo, Q. An, Z. Zhang, H. Liu, and D. Zhang, "Lattice Boltzmann method for simulation of solid-liquid conjugate boiling heat transfer surface with mixed wettability structures," *Phys. Fluids* **34**, 053305 (2022).
- <sup>5</sup>G. Son and V. K. Dhir, "Numerical simulation of film boiling near critical pressures with a level set method," *J. Heat Transfer* **120**, 183 (1998).
- <sup>6</sup>S. W. J. Welch and J. Wilson, "A volume of fluid based method for fluid flows with phase change," *J. Comput. Phys.* **160**, 662 (2000).
- <sup>7</sup>C. R. Kharangate and I. Mudawar, "Review of computational studies on boiling and condensation," *Int. J. Heat Mass Transfer* **108**, 1164 (2017).
- <sup>8</sup>H. Liu, A. J. Valocchi, and Q. Kang, "Three-dimensional lattice Boltzmann model for immiscible two-phase flow simulations," *Phys. Rev. E* **85**, 046309 (2012).
- <sup>9</sup>W. Z. Fang, L. Chen, Q. J. Kang, and W. Q. Tao, "Lattice Boltzmann modeling of pool boiling with large liquid-gas density ratio," *Int. J. Therm. Sci.* **114**, 172 (2017).
- <sup>10</sup>Q. Li, P. Zhou, and H. J. Yan, "Improved thermal lattice Boltzmann model for simulation of liquid-vapor phase change," *Phys. Rev. E* **96**, 063303 (2017).
- <sup>11</sup>H. Huang, M. Sukop, and X. Lu, *Multiphase Lattice Boltzmann Methods: Theory and Application* (John Wiley and Sons, Hoboken, 2015).
- <sup>12</sup>Q. Li, K. H. Luo, Q. J. Kang, Y. L. He, Q. Chen, and Q. Liu, "Lattice Boltzmann methods for multiphase flow and phase-change heat transfer," *Prog. Energy Combust. Sci.* **52**, 62 (2016).
- <sup>13</sup>X. Shan and H. Chen, "Lattice Boltzmann model for simulating flows with multiple phases and components," *Phys. Rev. E* **47**, 1815 (1993).
- <sup>14</sup>Q. Li, Q. J. Kang, M. M. Francois, Y. L. He, and K. H. Luo, "Lattice Boltzmann modeling of boiling heat transfer: The boiling curve and the effects of wettability," *Int. J. Heat Mass Transfer* **85**, 787 (2015).
- <sup>15</sup>Y. T. Mu, L. Chen, Y. L. He, Q. J. Kang, and W. Q. Tao, "Nucleate boiling performance evaluation of cavities at mesoscale level," *Int. J. Heat Mass Transfer* **106**, 708 (2017).
- <sup>16</sup>M. J. Sayyari and J. A. Esfahani, "2D lattice Boltzmann investigation of saturated pool boiling using a tunable surface tension model: Prandtl number effects on film boiling," *Meccanica* **53**, 3301 (2018).
- <sup>17</sup>L. Zhang, T. Wang, Y. Jiang, S. Kim, and C. Guo, "A study of boiling on surfaces with temperature-dependent wettability by lattice Boltzmann method," *Int. J. Heat Mass Transfer* **122**, 775 (2018).
- <sup>18</sup>X. Chang, H. Huang, Y. P. Cheng, and X. Y. Lu, "Lattice Boltzmann study of pool boiling heat transfer enhancement on structured surfaces," *Int. J. Heat Mass Transfer* **139**, 588 (2019).
- <sup>19</sup>X. Ma and P. Cheng, "3D simulations of pool boiling above smooth horizontal heated surfaces by a phase-change lattice Boltzmann method," *Int. J. Heat Mass Transfer* **131**, 1095 (2019).
- <sup>20</sup>C. Zhang, L. Chen, W. Ji, Y. Liu, L. Liu, and W. Q. Tao, "Lattice Boltzmann mesoscopic modeling of flow boiling heat transfer processes in a microchannel," *Appl. Therm. Eng.* **197**, 117369 (2021).
- <sup>21</sup>J. Chen, S. Ahmad, W. Deng, J. Cai, and J. Zhao, "Micro/nanoscale surface on enhancing the microchannel flow boiling performance: A lattice Boltzmann simulation," *Appl. Therm. Eng.* **205**, 118036 (2022).
- <sup>22</sup>J. A. Huang, C. Bao, Z. Jiang, and X. Zhang, "A general approach of unit conversion system in lattice Boltzmann method and applications for convective heat transfer in tube banks," *Int. J. Heat Mass Transfer* **135**, 873 (2019).
- <sup>23</sup>S. S. Baakeem, S. A. Bawazeer, and A. A. Mohamad, "A novel approach of unit conversion in the lattice Boltzmann method," *Appl. Sci.* **11**, 6386 (2021).
- <sup>24</sup>Y. L. He, Y. Wang, and Q. Li, *Lattice Boltzmann Method: Theory and Applications* (Science Press, Beijing, 2009) (in Chinese).
- <sup>25</sup>P. Yuan and L. Schaefer, "Equations of state in a lattice Boltzmann model," *Phys. Fluids* **18**, 042101 (2006).
- <sup>26</sup>Z. X. Tong, M. J. Li, and D. Li, "Coupling molecular dynamics and pseudopotential lattice Boltzmann method with nonideal equation of state for microscopical fluid flows," *Heat Transfer Res.* **53**, 33 (2022).
- <sup>27</sup>A. Jaramillo, V. P. Mapelli, and L. Cabezas-Gómez, "Pseudopotential lattice Boltzmann method for boiling heat transfer: A mesh refinement procedure," *Appl. Therm. Eng.* **213**, 118705 (2022).
- <sup>28</sup>L. S. Luo, W. Liao, X. Chen, Y. Peng, and W. Zhang, "Numerics of the lattice Boltzmann method: Effects of collision models on the lattice Boltzmann simulations," *Phys. Rev. E* **83**, 056710 (2011).
- <sup>29</sup>Q. Li and K. H. Luo, "Achieving tunable surface tension in the pseudopotential lattice Boltzmann modeling of multiphase flows," *Phys. Rev. E* **88**, 053307 (2013).
- <sup>30</sup>Y. H. Qian, D. D'Humières, and P. Lallemand, "Lattice BGK models for Navier-Stokes equation," *Europhys. Lett.* **17**, 479 (1992).
- <sup>31</sup>P. Lallemand and L. S. Luo, "Theory of the lattice Boltzmann method: Dispersion, dissipation, isotropy, Galilean invariance, and stability," *Phys. Rev. E* **61**, 6546 (2000).
- <sup>32</sup>Q. Li, K. H. Luo, and X. J. Li, "Lattice Boltzmann modeling of multiphase flows at large density ratio with an improved pseudopotential model," *Phys. Rev. E* **87**, 053301 (2013).

- <sup>33</sup>Z. Guo, C. Zheng, and B. Shi, "Discrete lattice effects on the forcing term in the lattice Boltzmann method," *Phys. Rev. E* **65**, 046308 (2002).
- <sup>34</sup>X. Shan, "Analysis and reduction of the spurious current in a class of multi-phase lattice Boltzmann models," *Phys. Rev. E* **73**, 047701 (2006).
- <sup>35</sup>X. Shan, "Pressure tensor calculation in a class of nonideal gas lattice Boltzmann models," *Phys. Rev. E* **77**, 066702 (2008).
- <sup>36</sup>Q. Li, Y. Yu, and Z. X. Wen, "How does boiling occur in lattice Boltzmann simulations?," *Phys. Fluids* **32**, 093306 (2020).
- <sup>37</sup>S. Gong and P. Cheng, "Lattice Boltzmann simulation of periodic bubble nucleation, growth and departure from a heated surface in pool boiling," *Int. J. Heat Mass Transfer* **64**, 122 (2013).
- <sup>38</sup>L. Fei, J. Yang, Y. Chen, H. Mo, and K. H. Luo, "Mesoscopic simulation of three-dimensional pool boiling based on a phase-change cascaded lattice Boltzmann method," *Phys. Fluids* **32**, 103312 (2020).
- <sup>39</sup>D. Albernaz, M. Do-Quang, and G. Amberg, "Multirelaxation-time lattice Boltzmann model for droplet heating and evaporation under forced convection," *Phys. Rev. E* **91**, 043012 (2015).
- <sup>40</sup>L. Fei, F. Qin, G. Wang, K. H. Luo, D. Derome, and J. Carmeliet, "Droplet evaporation in finite-size systems: Theoretical analysis and mesoscopic modeling," *Phys. Rev. E* **105**, 025101 (2022).
- <sup>41</sup>C. K. Law, "Recent advances in droplet vaporization and combustion," *Prog. Energy Combust. Sci.* **8**, 171 (1982).
- <sup>42</sup>G. Zhao-Li, Z. Chu-Guang, and S. Bao-Chang, "Non-equilibrium extrapolation method for velocity and pressure boundary conditions in the lattice Boltzmann method," *Chin. Phys.* **11**, 366 (2002).
- <sup>43</sup>A. Hu and D. Liu, "2D simulation of boiling heat transfer on the wall with an improved hybrid lattice Boltzmann model," *Appl. Therm. Eng.* **159**, 113788 (2019).
- <sup>44</sup>C. Zhang, F. Hong, and P. Cheng, "Simulation of liquid thin film evaporation and boiling on a heated hydrophilic microstructured surface by lattice Boltzmann method," *Int. J. Heat Mass Transfer* **86**, 629 (2015).
- <sup>45</sup>J. Qin, Z. Xu, and X. Ma, "Pore-scale simulation on pool boiling heat transfer and bubble dynamics in open-cell metal foam by lattice Boltzmann method," *J. Heat Transfer* **143**, 011602 (2021).
- <sup>46</sup>S. Ahmad, J. Chen, C. Eze, and J. Zhao, "Lattice Boltzmann study of nucleation site interaction and nucleate boiling heat transfer on a hybrid surface with multiple cavity-pillar structures," *Int. J. Therm. Sci.* **163**, 106860 (2021).
- <sup>47</sup>K. Mondal and A. Bhattacharya, "Pool boiling enhancement through induced vibrations in the liquid pool due to moving solid bodies—A numerical study using lattice Boltzmann method (LBM)," *Phys. Fluids* **33**, 093310 (2021).
- <sup>48</sup>S. Gong and P. Cheng, "Numerical simulation of pool boiling heat transfer on smooth surfaces with mixed wettability by lattice Boltzmann method," *Int. J. Heat Mass Transfer* **80**, 206 (2015).
- <sup>49</sup>E. W. Lemmon, I. H. Bell, M. L. Huber, and M. O. McLinden, *Thermophysical Properties of Fluid Systems* (National Institute of Standards and Technology, Gaithersburg, MD, 2022).
- <sup>50</sup>Y. Yu, Q. Li, Z. X. Wen, and R. Z. Huang, "Investigation on boundary schemes in lattice Boltzmann simulations of boiling heat transfer involving curved surfaces," *Phys. Fluids* **32**, 063305 (2020).
- <sup>51</sup>R. Mei, L. S. Luo, and W. Shyy, "An accurate curved boundary treatment in the lattice Boltzmann method," *J. Comput. Phys.* **155**, 307 (1999).
- <sup>52</sup>Y. Y. Hsu, "On the size range of active nucleation cavities on a heating surface," *J. Heat Transfer* **84**, 207 (1962).
- <sup>53</sup>S. M. Ghiaasiaan, *Two-Phase Flow, Boiling, and Condensation: In Conventional and Miniature Systems* (Cambridge University Press, 2017).